Particle Size Effect on the Film-Forming Process of PS/PBA Composite Latexes

Şaziye Uğur,[1] M. Selin Sunay,[1] Abdelhamid Elaissari,[2] Önder Pekcan[3]
[1]*Department of Physics, Istanbul Technical University, Maslak 34469, Istanbul, Turkey*

[2]*LAGEP Laboratory, Claude Bernard University, Bât. CPE-308G, 43 Boulevard du 11 novembre 1918, 69622 Villeurbanne Cedex, France*

[3]*Kadir Has University, Faculty of Arts and Science, Cibali 34230, Istanbul, Turkey*

In this work, the effect of hard particle size and blend ratio on the film formation behavior of hard polystyrene (PS) and soft poly(*n*-butyl acrylate) (PBA) latex blends was studied by means of steady-state fluorescence and UV–visible techniques in conjunction with atomic force microscopy. Three different sets of latexes were synthesized: PBA latex (diameter 97 nm), pyrene (P)-labeled large PS (LgPS; diameter 900 nm), and small PS (SmPS; diameter 320 nm). Two different series of latex blends (LgPS/PBA and SmPS/PBA) were prepared with varying blend composition at room temperature separately. Films were then annealed at elevated temperatures above glass transition (T_g) temperature of PS. Fluorescence intensity (I_P) from P and photon transmission intensity (I_{tr}) were measured after each annealing step to monitor the stages of film formation. The results showed that a significant change occurred in I_P and I_{tr} at a certain critical weight fraction (R_c) of PBA. Below R_c, two distinct film formation stages, which are named as void closure and interdiffusion, were seen. However, at PBA concentrations nearer to or above R_c, no film formation can be achieved. Comparing to the LgPS/PBA, the sintering process of SmPS/PBA particles occurred at much lower temperatures. Film formation stages for $R < R_c$ were modeled, and related activation energies were calculated. Void closure (ΔH) and interdiffusion (ΔE) activation energies for SmPS/PBA were also found smaller in comparing with LgPS/PBA series. However, ΔH and ΔE values were not changed much with the blend composition for both series. POLYM. COMPOS., 31:1637–1652, 2010. © 2009 Society of Plastics Engineers

INTRODUCTUON

Waterborne organic coatings are gaining importance because of the use of water as a "solvent" instead of volatile organic compounds (VOCs). The formation of a dry film from an aqueous colloidal suspension of polymer particles takes places in different stages [1, 2]. Colloidal particles with glass transition temperature (T_g) above the drying temperature are named as hard latex (high-T_g) particles. On the other hand, colloidal particles with T_g below the drying temperature are called as soft latex (low-T_g) particles. Traditionally, the film formation process of polymer latex is considered in terms of three sequential steps: (i) water evaporation and subsequent packing of polymer particles; (ii) deformation of the particles and close contact between the particles if their T_g is less than or close to the drying temperature (soft latex). Hard latex (high-T_g) stays undeformed at this stage. In the annealing of high hard latex system, deformation of particles first leads to void closure [3–6] and then after the voids disappear, diffusion across particle–particle boundaries starts, that is, the mechanical properties of hard latex films evolve during annealing after all solvent has evaporated and all voids have disappeared; (iii) coalescence of the deformed particles to form a homogeneous film [2] where macromolecules belonging to different particles mix by interdiffusion [7, 8].

In most of the previous studies, the kinetics of film formation have been conducted on a single-component latex. Dry films of such polymers have poor mechanical properties [2, 9, 10]. For example, low-T_g lattices have good film-forming abilities. They are easily deformed and yield excellent film formation properties. However, the film produced will be often tacky, have poor mechanical properties and solvent resistance. High-T_g polymers yield particles that do not deform easily and they require to add VOCs to the dispersion. Their role is to act as transient plasticizers, promoting both particle deformation and healing of the interparticle interface during the film formation. To get films with good mechanical and barrier properties, composite latex systems involving two or more different

Correspondence to: Şaziye Uğur; e-mail: saziye@itu.edu.tr
Contract grant sponsor: TUBITAK-1001 Research Project; contract grant number: 107T394.
DOI 10.1002/pc.20954
View this article online at wileyonlinelibrary.com.

polymer compositions can be used [10–12]. One approach to do this is the use of structured core/shell latex particles [13–16] that have a high-Tg polymer core and a low-T_g film-forming polymer shell [13–16] as equivalent to an elastomeric matrix containing rigid inclusions. Another way is the physical blending of two separate latex dispersions with homogeneous particle morphologies. It is envisioned that low-T_g latex will film-form to create a continuous phase to which the other high-T_g latex will impart desirable mechanical or optical properties and that good film formers [17]. Such latex blends would not require volatile solvent plasticizers and therefore be less damaging to the environment. Thus, the combination of soft (low-T_g) and hard (high-T_g) lattices has become an area of specific scientific and technical interest [9, 10, 14–21].

Within the past several years, the use of latex blends has gained increased attention in the literature [2], which reflects an even greater amount of study in industry. One of the main interests in latex blends is the drive toward zero-VOCs in the organic coating industry [22]. The research by Winnik and Feng [10] has shown that hard/soft latex blends can be used to achieve films that produce lower levels of VOC and thus are less damaging to human health and the environment. Parameters affecting the mechanical properties of such blends are the properties of the neat constituents, the composition, the particle sizes, the particle size ratio (D_{soft}/D_{hard}), the morphology, and interfacial interactions. Eckersley and Helmer [19] have demonstrated that careful control of large/small size ratio and hard/soft concentration ratio can produce composite films with desired film formation characteristics and also with enhanced blocking resistance and mechanical properties. Latex dispersions with controlled particle size distributions have been devised so as to increase the solids content and thereby minimize solvent usage while gaining additional control of viscosity [23]. As the viscosity of a colloidal dispersion depends on the particle size [24], the control of particle size distribution has a pronounced effect on the rheology of latex dispersions.

Bimodal particle size distribution is gaining attention because of their potential to enable control of the dispersion rheology, the film formation characteristics, and the final film properties. The influence of particle size and particle size ratio on the morphology and the mechanical properties of 50/50 blends of hard poly(methyl methacrylate-*co*-styrene) and soft poly(methyl methacrylate-*co*-butyl acrylate) has been studied by Colombini et al. [18, 25]. The enhancement of the mechanical properties at temperatures between the two glass transitions of the neat constituents was particularly influenced by the particle size of the hard phase. The reason for this behavior was the existence of a critical volume fraction at which the hard particles prevented the soft particles from forming a continuous stable film, and this behavior is related to particle size, particle size ratio, and volume fraction. Larger particle size ratios and lower critical volume fractions of hard particles lead to percolation and aggregation [19], a phenomenon that has been observed by TEM micrographs [18]. Colombini et al. [25] also studied the influence of thermal annealing on 50/50 latex blends and found that the morphology of the films changed drastically at temperatures above the glass transition temperature of the hard latex as a result of the hard particles coalescing and forming a cocontinuous phase with the soft phase. Geurts et al. [26] have pointed out, particle packing can be affected by particle stability and the clustering of particles of the same size.

TABLE 1. Properties of the neat latexes.

Latex	Abbreviation	Particle size (nm)	M_w (g/mol)	M_w/M_n	T_g (°C)
PS particle (large)	LgPS	900	8.50×10^4	3.60	105
PS particle (small)	SmPS	320	8.61×10^4	4.26	105
PBA particle	PBA	97	–	–	−41

The aim of this work was to study the influence of hard/soft latex fraction and hard particle size on the morphology and film formation behaviors of PS/PBA latex blends. To investigate the effect of hard latex particle size on film formation properties of PS/PBA blends, two series of blends were prepared for two different hard PS particle with 900 nm (LgPS) and 320 nm (SmPS) in diameters. Within these two series, the blend compositions have been kept identical, only the particle size of the hard latex was changed. Therefore, the differences in the experimental data for two series result from the difference in the hard PS particle size in PS/PBA latex blends. Such blend systems can therefore be viewed as suitable models for studying the influence of both the hard/soft blend composition and the hard particle size on the film formation behavior of latex blends.

EXPERIMENTAL

Latex Preparation

Hard PS Latexes. Two different hard polystyrene (PS) latexes with different sizes were synthesized. Fluorescent PS latexes were produced via a surfactant-free emulsion polymerization [27] process. Styrene monomer (99% pure from Janssen) was first introduced in the reactors containing boiled and deionized water, and the fluorescent monomer 1-pyrenylmethyl methacrylate (PolyFluor™ 394 from Polyscience) was first dissolved in small amount of styrene. The water-soluble radical initiator potassium persulfate was dissolved in water and added when the polymerization temperature was equilibrated at 70°C.

Soft PBA Latex. The soft latex samples are composed of poly(*n*-butyl acrylate) (PBA) and were prepared by semicontinuous process [28]. All reagents were from Merck (Darmstadt, Germany). Monomers: *n*-butyl acrylate

DOI 10.1002/pc

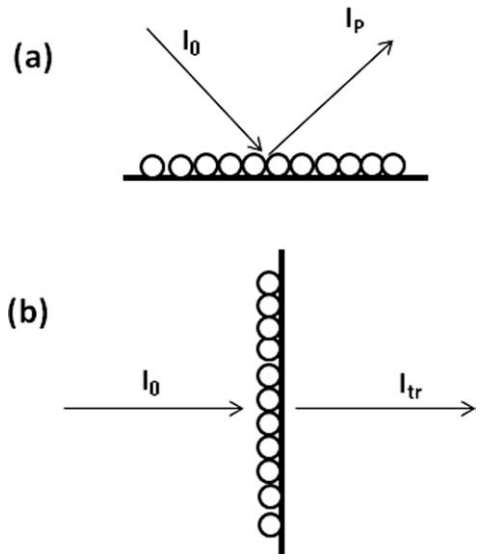

FIG. 1. Schematic illustration of sample position and (a) incident light (I_0) and emission (I_P) intensities, (b) transmitted light intensity (I_{tr}).

(BA) and acrylic acid (AA) were purified by filtration through basic alumina powder. The surfactant, sodium dodecyl sulfate (purity over 99%), and initiator, ammonium persulfate ($(NH_4)_2S_2O_8$) (purity 99%), were used directly from the bottle. The reaction temperature was adjusted to 75°C for 3 h and then to 82°C for 2 h. The synthesized core-shell lattice is composed of BA (99 wt%) and a small percentage of acrylate acid (1 wt%) [29]. They are fairly monodisperse, having all very similar mean diameters (97 nm), and has a T_g (=−41°C) below room temperature. Furthermore, the AA is well incorporated and a large majority of it is located in the particle shell [28].

The properties of the three prepared latexes and their abbreviations are displayed in Table 1. Particle size and its distribution were determined by atomic force microscopic (AFM) observation. The molecular weights of individual PS chain (M_w) were measured by gel permeation chromatography.

Film Preparation

Table 1 provides some characteristics of the three parent latex dispersions used in making the latex blends. Two parameters of particular relevance to this study are the particle size and the glass transition temperature. The polymers with a glass transition temperature (T_g) of −41°C are referred to here as "soft," and we refer to the high-T_g particles (105°C) as "hard." Blend films were prepared by mixing different fractions (by weight) of the hard PS and soft PBA dispersions. As our aim is to study the particle size effect of hard latex on film formation behavior of hard/soft latex composite, we prepared two series of blends; Series 1: large-hard PS and soft PBA (LgPS/PBA); Series 2: small-hard PS and soft PBA (SmPS/PBA).

We will refer to the particle types using the abbreviations shown in Table 1 and in parentheses above. Hard/soft latex blends were prepared by mixing hard/soft lattices with the following weight compositions for each series: 100/0, 80/20, 60/40, 50/50, 30/70, 20/80, and 10/90. The blends were stirred continuously for at least 1 h to ensure a uniform dispersion. Then, these dispersions were cast into glass plates with similar surface areas (0.8 × 2.5 cm^2) and allowed to dry under the ambient conditions of the laboratory. After drying, samples were separately annealed above T_g of PS for 10 min at temperatures ranging from 100 to 250°C. The temperature was

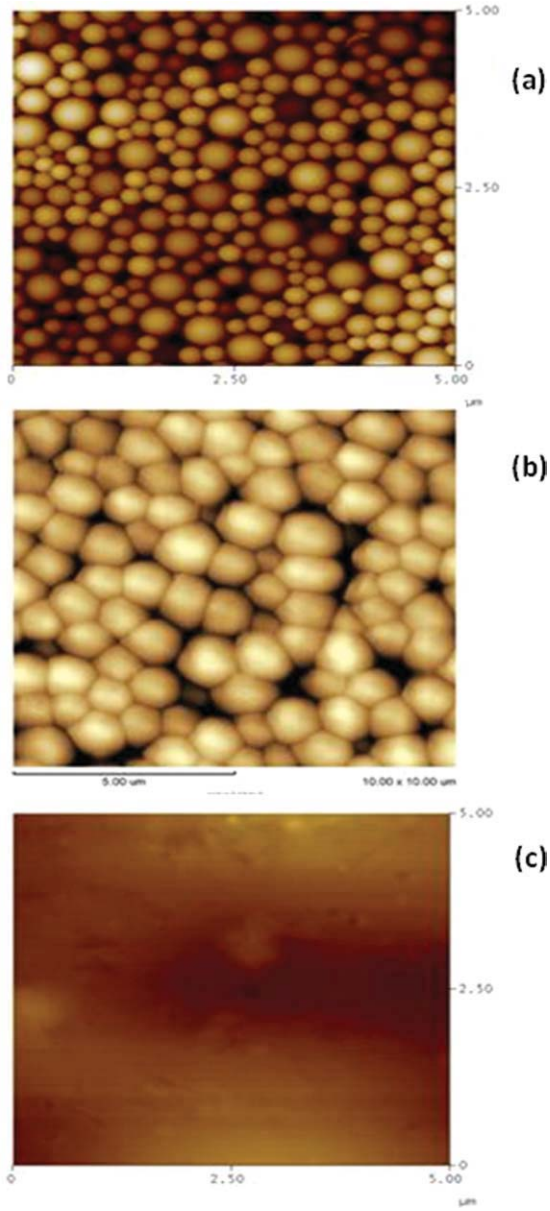

FIG. 2. Atomic force microscopy (AFM) images of neat (a) SmPS, (b) LgPS, and (c) PBA latexes produced for this study. [Color figure can be viewed in the online issue, which is available at wileyonlinelibrary.com.]

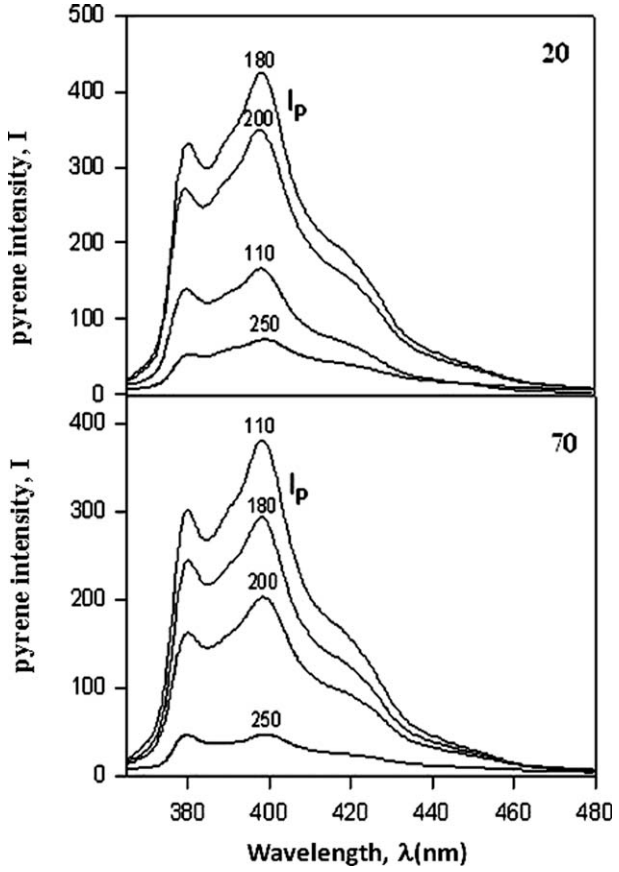

FIG. 3. Fluorescence emission spectra from SmPS/PBA blend films for 20 and 70 wt% PBA content after being annealed at various temperatures for 10 min. Numbers on each curve represent annealing temperature.

maintained within $\pm 2^{\circ}$C during annealing. After each annealing step, films were removed from the oven and cooled down to room temperature. The film thickness of the presented blend films was determined to be 20 μm in average. The data reported in this article correspond to the average from a set of five measurements.

Methods

Fluorescence Measurements. After annealing at room temperature, each sample in both series was placed in the solid surface accessory of a Perkin-Elmer Model LS-50 fluorescence spectrometer. Pyrene (P) was excited at 345 nm and fluorescence emission spectra were detected between 360 and 600 nm. All measurements were performed in the front-face position at room temperature. Slit widths were kept at 8 nm during all steady-state fluorescence (SSF) measurements. The sample position, incident light, I_0, and I_P emission intensities are shown in Fig. 1a.

Photon Transmission Measurements. Photon transmission experiments were performed using Variant Carry-100 UV–visible (UVV) spectrometer. The transmittances of the films were detected at 500 nm. A glass plate was used as a standard for all UVV experiments, and measurements were performed at room temperature after each annealing processes. The sample position and the transmitted light intensity, I_{tr}, are presented in Fig. 1b.

Atomic Force Microscopy Measurements. Micrographs of the blend films were recorded with SPM-9500-J3 Shimadzu and NanoScope (R) IIIa multimode scanning probe atomic force microscopies. At least three different regions of each surface were imaged to verify reproducibility and to ensure that a truly representative image was obtained. The results were also reproduced for up to three different samples prepared separately. Figure 2a–c shows AFM images of individual SmPS, LgPS, and PBA latex components produced for this study before annealing. In Fig. 2a and b, both hard SmPS and LgPS particles not seem to deform keeping their original (spherical) shapes and form a film with rough surface. However, AFM image of pure PBA film (Fig. 2c) reveals an overall flat and smooth film surface. These particles are film forming at room temperature and form continuous, void-free films because of their low-T_g ($=-41^{\circ}$C).

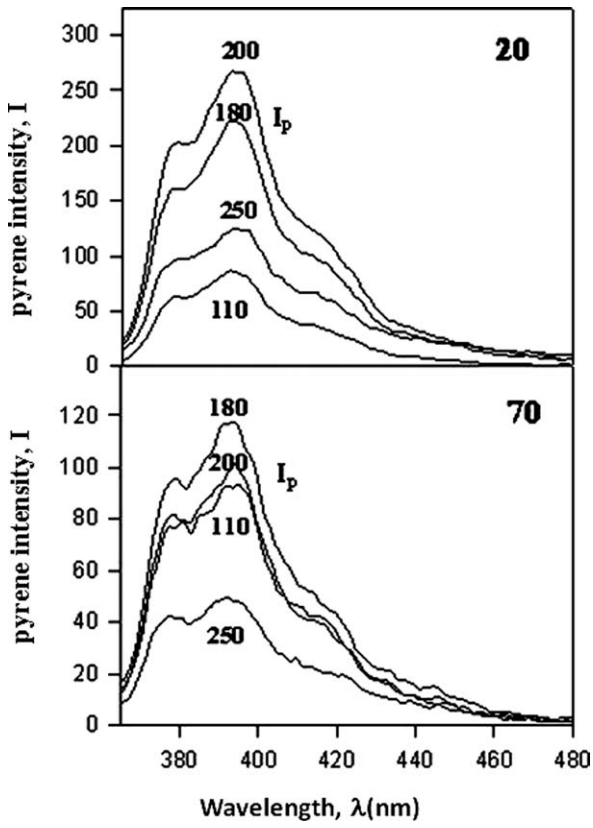

FIG. 4. Fluorescence emission spectra from LgPS/PBA blend films for 20 and 70 wt% PBA content after being annealed at various temperatures for 10 min. Numbers on each curve represent annealing temperature.

DOI 10.1002/pc

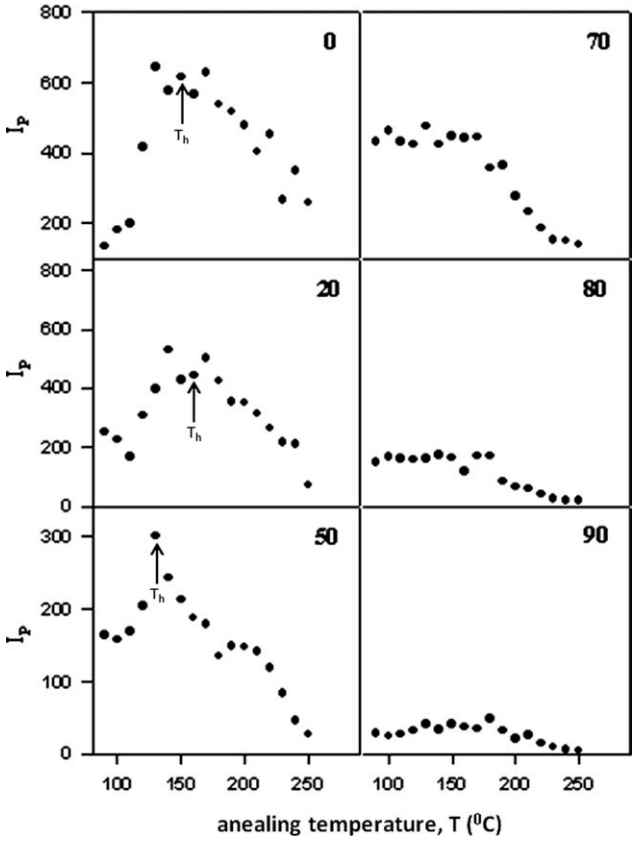

FIG. 5. Plot of fluorescence intensities, I_P versus annealing temperature, T for the SmPS/PBA blend films contain different amount of PBA. Numbers on each curve represent PBA content in the film. Here, T_h is the healing temperature.

RESULTS AND DISCUSSION

Fluorescence emission spectra of 20 and 70 wt% PBA content blend films for both SmPS/PBA and LgPS/PBA series annealed at various temperatures for 10 min are shown in Figs. 3 and 4, respectively. As the annealing temperature is increased, fluorescence intensity, I_P, from the blend films with 20 wt% PBA content first increased and then decreased with increasing annealing temperatures for Series 1 (see Fig. 3). However, for the 70 wt% PBA content blend film, I_P intensity decreased with annealing temperature. On the other hand, in Fig. 4 (Series 2), the I_P intensity for both 20 and 70 wt% PBA content films behaves in the same way, that is, first increased and then decreased with annealing. The plots of I_P versus annealing temperature, T for 0, 20, 50, 70, 80, and 90 wt% PBA content blend films for both series are shown in Figs. 5 and 6, respectively. It is seen that I_P intensity from blends with 0–50 wt% PBA content for Series 1 (see Fig. 5) and 0–70 wt% PBA content for Series 2 (see Fig. 6) first increases by showing a maximum at a certain temperature called healing temperature, T_h. Then, because of further annealing, I_P decreases. The increase and decrease of I_P upon annealing of these blend films can be explained with the void closure and interdiffusion processes, respectively [29, 30]. However, I_P intensity from blends which have 70–90 wt% PBA for Series 1 (see Fig. 5) and 80–90 wt% PBA for Series 2 (see Fig. 6) behaves quite differently. In other words, I_P intensities from the blends prepared with low PS content are weak and almost remain unchanged during annealing, indicating that no film formation process takes place in a traditional way, that is, because of its low-T_g, PBA latexes have already accomplished their film formation process.

The change in transmittance of the blend films upon annealing for SmPS/PBA and LgPS/PBA series is shown in Figs. 7 and 8 with increasing (0, 20, 50, 70, 80, and 90 wt%) PBA component. I_{tr} presents a dramatic increase above a certain temperature called minimum film formation temperature, T_0 above a certain amount of PBA for both series. I_{tr} increases reaching a maximum and then remains constant for 0–50 wt% PBA content blend films (Series 1) and 0–70 wt% PBA content blend films (Series 2) with annealing. The increase in I_{tr} with annealing temperature primarily due to the closure of voids [29–31] between PS particles by viscous flow in these films. However, above these ranges of PBA, I_{tr} almost does not

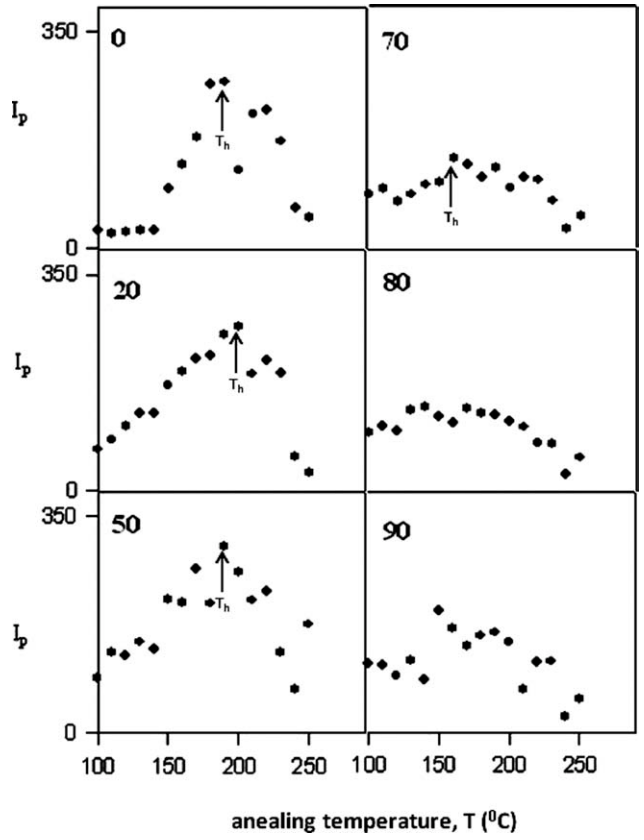

FIG. 6. Plot of fluorescence intensities, I_P versus annealing temperature, T for the LgPS/PBA blend films contain different amount of PBA. Numbers on each curve represent PBA content in the film. Here, T_h is the healing temperature.

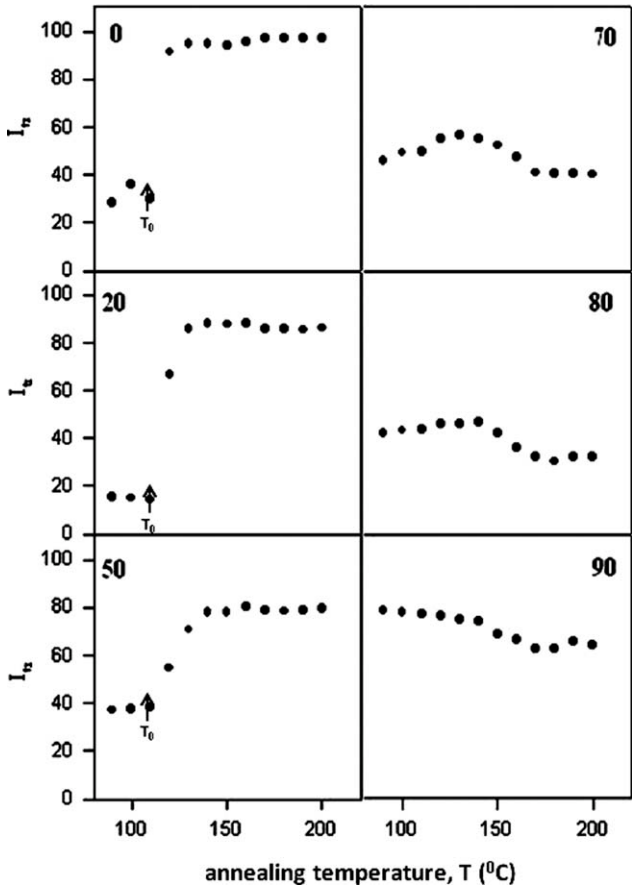

FIG. 7. Plot of I_{tr} versus annealing temperatures for SmPS/PBA series contain various amount of PBA. Numbers on each curve represent PS content in the film. T_0 is the minimum film formation temperature.

change with annealing temperature for both series. It means that these curves present no void closure phenomenon in consistent with the fluorescence results. Film formation process has already been accomplished due to PBA's low-T_g character.

Here, it has to be noted that all the films produced from blends of SmPS/PBA particles are optically more transparent than those produced from LgPS/PBA particles at all annealing temperatures. Optical transmission measurements are a measure of the number and size of air voids in a polymer film [32]. Nevertheless, optical transmissivity can be qualitatively [32] related to void size and concentration for these films. Regardless of the void fraction, transmission decreases with increasing void radius. Here, despite the refractive indices of two polymers are somewhat different [33] (with differences of about 0.12), we suggest that the turbidity (or low I_{tr}) at low annealing temperatures is mostly associated with aggregation [34] of hard latex and voids [10, 29, 30, 35] in the films which can scatter the light. It is understood that the overall fraction of voids in the SmPS/PBA blend film is much lower than in LgPS/PBA blend films. Drawing upon the AFM results shown in following section, we can conclude that although the void concentration is high, high transparency is achieved from the void size being small. However, clustering between LgHd particles creates interparticle voids relatively large in size that are filled extremely slowly by a soft polymer matrix. AFM micrographs of these films indicate an increasing void fraction (more and/or larger voids being present) with an increase of the PBA phase. They therefore scatter light significantly, so that the optical transmission is reduced with increasing both void concentration and void size. We will discuss later how the optical transparency of the LgPS/PBA blend is reduced in comparison to the SmPS/PBA blend. Thus, latex blends that contain polymer particles with the same glass transition temperature and presumably the same mechanical properties but with different sizes (i.e., LgPS and SmPS) form films with differing void concentrations. Blends dominated with LgPS particles have a high void fraction, whereas films containing SmPS particles have a much lower void fraction, as seen in AFM images in the following section.

On the other hand, after annealing at 200°C, transparency of SmPS/PBA film is quite high (up to 80%) at 0–50 wt% PBA content. I_{tr} shows a sudden decrease (about 40%) at 70 wt% PBA and then increases again up to 80% for 90 wt% PBA. As the PS and PBA are indeed immiscible polymers, the decrease in I_{tr} can be explained

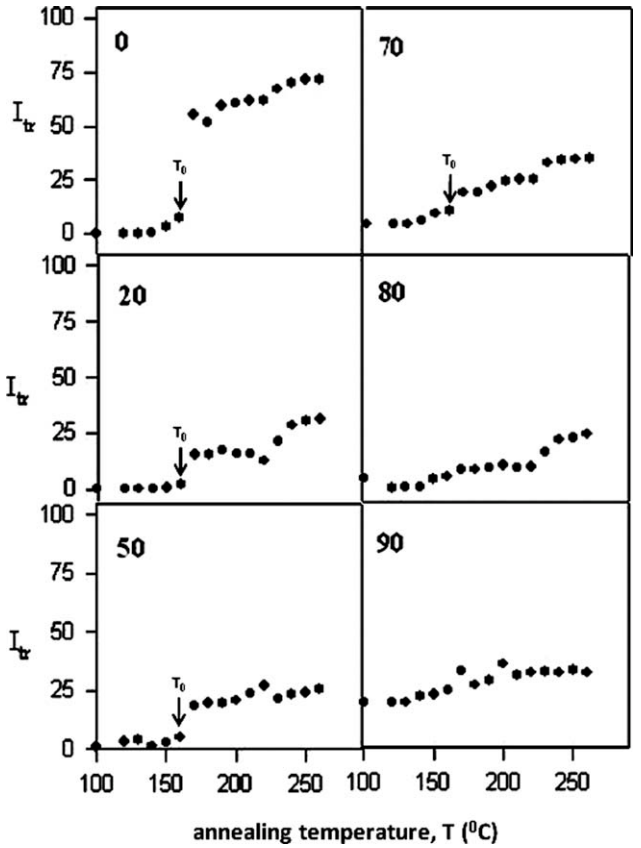

FIG. 8. Plot of I_{tr} versus annealing temperatures for LgPS/PBA series contain various amount of PBA. Numbers on each curve represent PS content in the film. T_0 is the minimum film formation temperature.

DOI 10.1002/pc

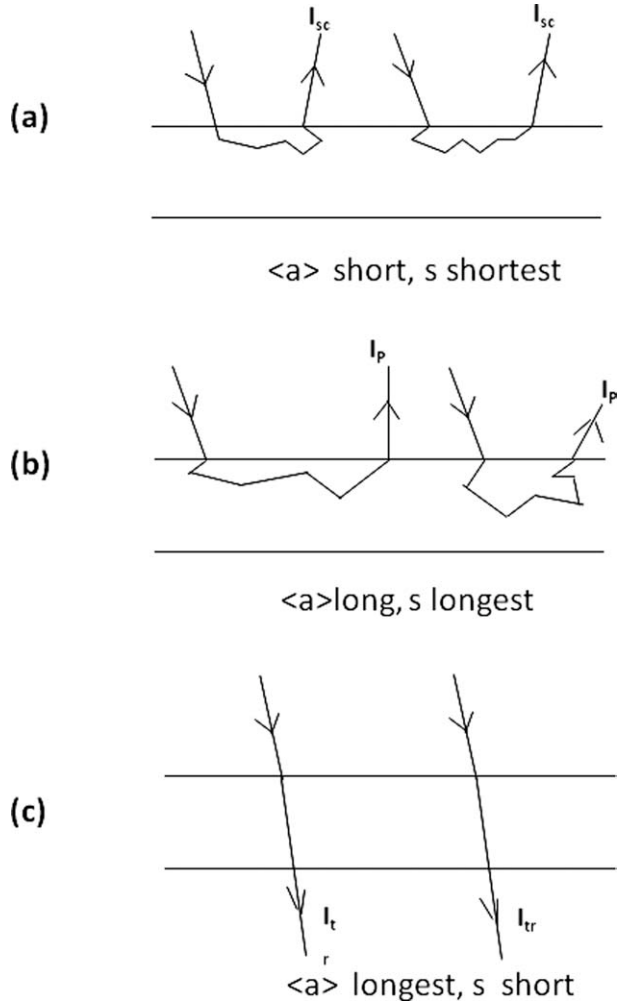

FIG. 9. Cartoon representation of film formation from polystyrene particles (a) before annealing, (b) film with no voids, (c) film with no particle–particle interfaces, and (d) film after interdiffusion process is completed.

with the phase separation process between two polymers during coalescence of PS latexes due to the breakup and coarsening of the phase-separated domains. In this range, the structure of the film is made of individual coalesced PS domains immersed in a continuous matrix of PBA polymer. As the size of PS domains is large with respect to the wavelength of the visible light, they scatter the light that cause turbidity in the film [34]. Because of the continuous film formation, transparency is high for other SmPS/PBA blend films. On the other hand, films prepared from Series 2 (LgPS/PBA) have high transmission (up to 75%) only for pure LgPS (0 wt% PBA content) film. As the PBA phase is increased, the transmission decreases dramatically (around 30%) and almost does not change with increasing PBA content. As the domain sizes in LgPS/PBA blends are larger than those in SmPS/PBA blend films, the transparency is lower. Thus, it can be concluded that the PBA soft phase and the PS hard phase existed as two separate phases in these films as seen in AFM images in the following section.

The behavior of I_P in blend films for 0–50 wt% range of PBA (Series 1) and for 0–70 wt% range of PBA (Series 2) during annealing is schematically presented in Fig. 9a–c, respectively. The variation in I_P depends on optical path, s, of a photon in the blend [29, 30]. This optical path is directly proportional to the probability of a photon encountering a pyrene molecule. In Fig. 9a, as the film possesses many voids, the photon is scattered from the particle surface, which results in short mean free ($<a>$) and optical path (s) yielding very low I_P. Figure 9b shows a film in which interparticle voids disappear because of annealing giving rise to a long mean free ($<a>$) and optical path, s, in the film. Clearly, in this regime, with the same number of rescatterings, a photon

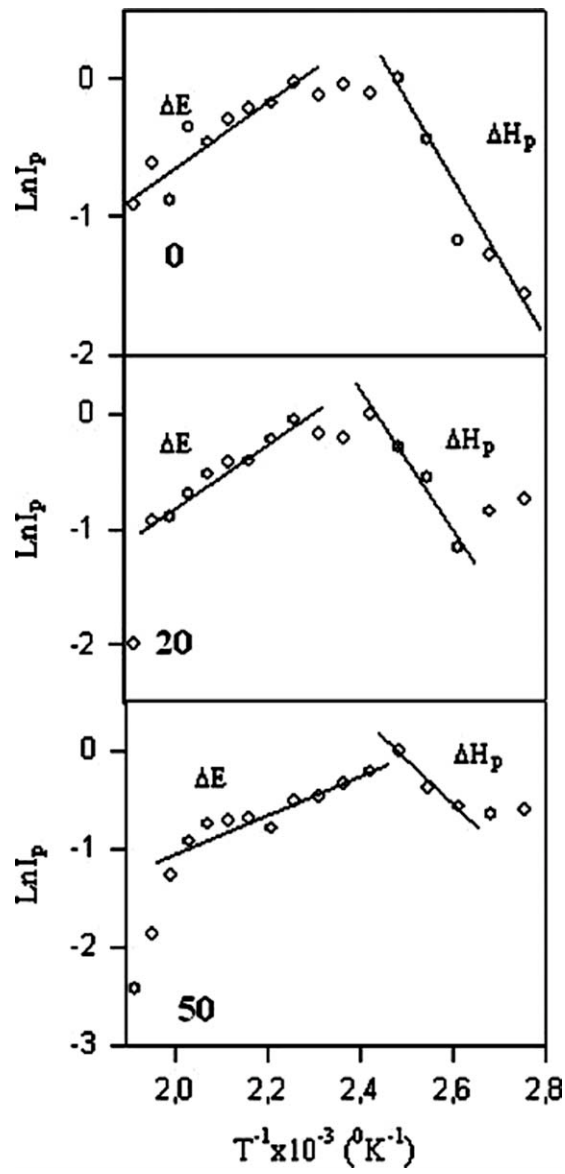

FIG. 10. Logarithmic plots of I_P data in Fig. 5 versus inverse of annealing temperatures (T^{-1}) for the films annealed at 10 min time intervals. The slope of the linear relations produces ΔH_P and ΔE values, listed in Table 2.

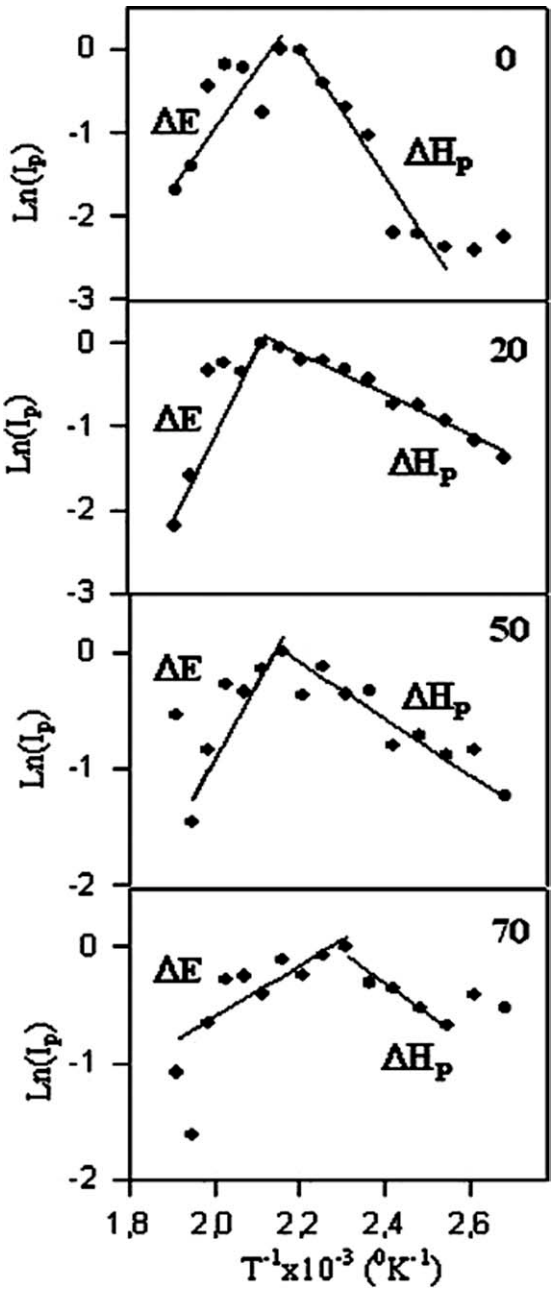

FIG. 11. Logarithmic plots of I_P data in Fig. 6 versus inverse of annealing temperatures (T^{-1}) for the films annealed at 10 min time intervals. The slope of the linear relations produces ΔH_P and ΔE values, listed in Table 2.

will spend some time in the blend, and, consequently, I_P values are large. Because of the further annealing (Fig. 9c), the blend starts to become essentially transparent to the photon, the mean free path diverges, and s eventually becomes short, that is, of the order of the blend thickness, d. Hence, the decrease in I_P after complete annealing has occurred.

The increase in I_{tr} and I_p intensities in the 0–50 wt% PBA range for Series 1 and 0–70 wt% PBA range for Series 2 can be explained by void closure and surface smoothing with annealing. On the other hand, the increase in I_P presumably corresponds to the void closure process up to the T_h point where the healing process takes place [29, 30]. Decrease in I_P above T_h can be understood by interdiffusion between polymer chains. To understand these phenomena, the following mechanisms and their formulations are proposed.

Void Closure

Void closure kinetics can determine the activation energy for viscous flow during latex film formation. Mackenzie and Shuttleworth [5] modeled the void closure by viscous flow under the action of surface energy using the equation

$$\frac{dr}{dt} = -\frac{\gamma}{2\eta}\left(\frac{1}{\rho(r)}\right). \tag{1}$$

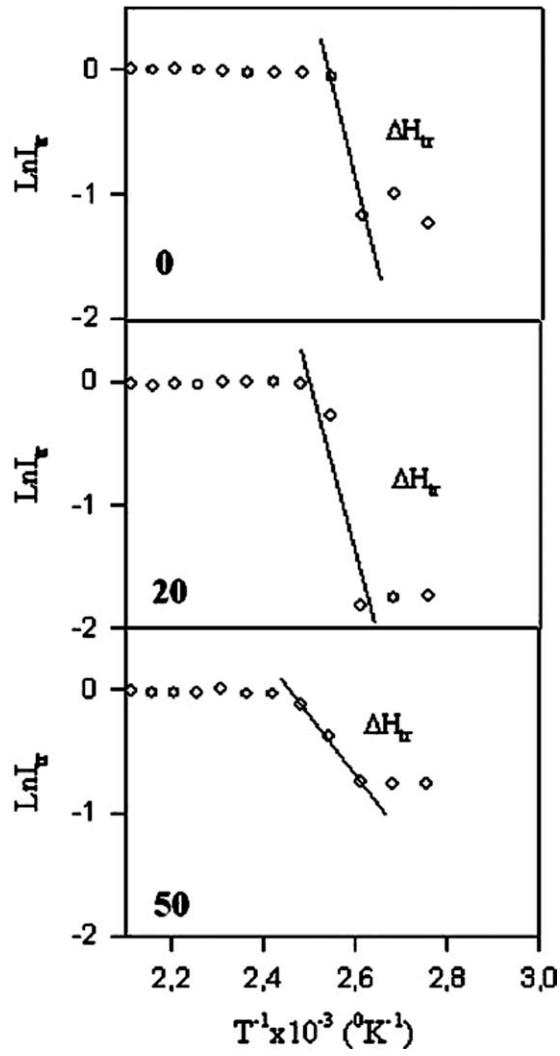

FIG. 12. Logarithmic plots of I_{tr} data in Fig. 7 versus inverse of annealing temperatures (T^{-1}) for the films annealed at 10 min time intervals. The slope of the linear relations produces ΔH_P and ΔE values, listed in Table 2.

DOI 10.1002/pc

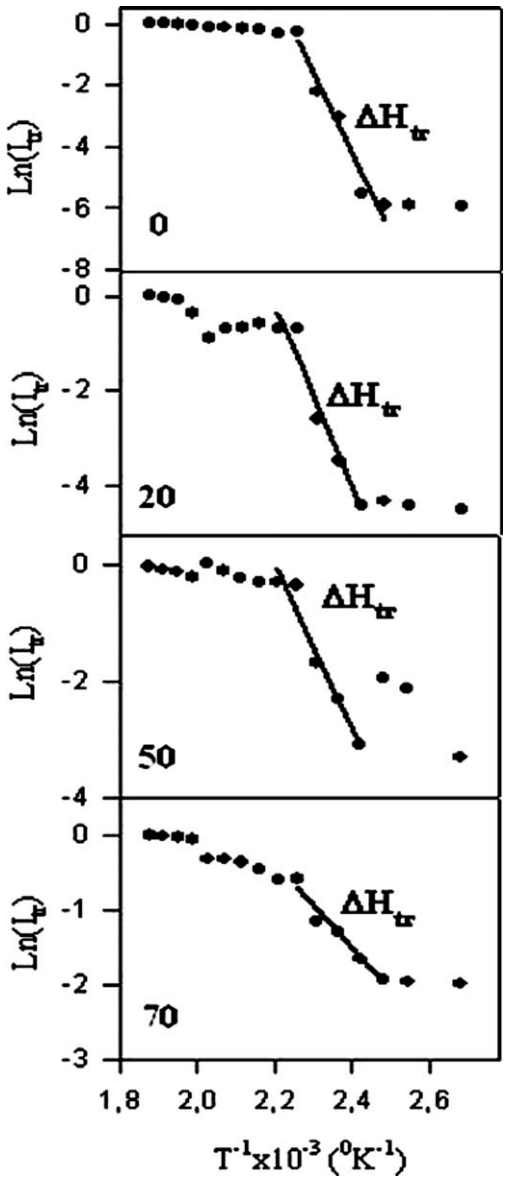

FIG. 13. Logarithmic plots of I_{tr} data in Fig. 8 versus inverse of annealing temperatures (T^{-1}) for the films annealed at 10 min time intervals. The slope of the linear relations produces ΔH_P and ΔE values, listed in Table 2.

This equation assumes that a spherical void of radius r shrinks as a function of time, where γ is the surface energy at the air/polymer interface, t is time, and $\rho(r)$ is the relative density. When the *Eq. 1* is integrated, the following relation can be written as follows:

$$t = \frac{2AC}{\gamma}\exp\left(\frac{\Delta H}{kT}\right)\left(\frac{1}{r^2} - \frac{1}{r_o^2}\right). \quad (2)$$

Here, C is a constant related to relative density $\rho(r)$. As we stated earlier, decrease in void size (r) causes an increase in both I_{tr} and I_P. If the assumption is made that I_{tr} and/or I_P ($=I$) is inversely proportional to the sixth power of void radius, r, then *Eq. 2* can be written as follows:

$$I(T) = S(t)\exp\left(-\frac{3\Delta H}{kT}\right), \quad (3)$$

where $S(t) = (\gamma t/2AC)^3$.

As it was already argued earlier that the increase in both I_P and I_{tr} originates because of the void closure process, then *Eq. 3* was applied to I_{tr} above T_0 and to I_P below maxima (below T_h) for all film samples in two series. Figures 10 and 11 present the LnI_P versus T^{-1}, and Figs. 12 and 13 present LnI_{tr} versus T^{-1} plots from which ΔH_P and ΔH_{tr} activation energies were obtained. The measured ΔH_P and ΔH_{tr} activation energies are listed in Table 2 for both series, where it is seen that activation energies do not change much, that is, the amount of heat which was required by 1 mol of polymeric material to accomplish a jump during viscous flow does not change by varying the blend composition in the films. ΔH_P values were found to be smaller than ΔH_{tr} values for both series. This difference most probably originates from different techniques; second one measures the film formation from the inner latexes, which requires higher energies. When comparing the activation energies of both series, it is seen that ΔH values of LgPS/PBA blends are larger than those of SmPS/PBA blends. This implies that the viscous flow process is significantly affected by the hard PS particle size. With smaller diameter (i.e., 320 nm), the SmPS particles have larger surface area or surface free energy. The driving force for film formation is proportional to the inverse of the particle size, according to the descriptions of film formation driven by capillary forces [2]. The greater curvature and higher surface area of small particles are expected to encourage film formation. The specific surface area or the total surface energy of SmPS particles (diameter 320 nm) is much larger than that of

TABLE 2. Activation energy values (ΔH_P, ΔH_{tr}, and ΔE) of both series.

	SmPS/PBA			LgPS/PBA		
PBA (%)	ΔH_P	ΔH_{tr}	ΔE	ΔH_P	ΔH_{tr}	ΔE
0	3.58	11.18	9.55	5.22	17.18	28.81
20	3.93	9.25	11.23	1.61	12.67	42.56
40	3.23	7.93	6.36	1.60	5.20	25.82
50	2.91	3.18	7.17	1.60	9.38	26.17
70	–	–	–	1.77	3.76	8.90

TABLE 3. Minimum film formation (T_0) and healing (T_h) temperatures for two blend series.

	SmPS/PBA		LgPS/PBA	
PBA (wt%)	T_0 (°C)	T_h (°C)	T_0 (°C)	T_h (°C)
0	110	150	160	190
20	110	160	160	200
40	110	130	150	190
50	110	130	160	190
70	–	–	140	170

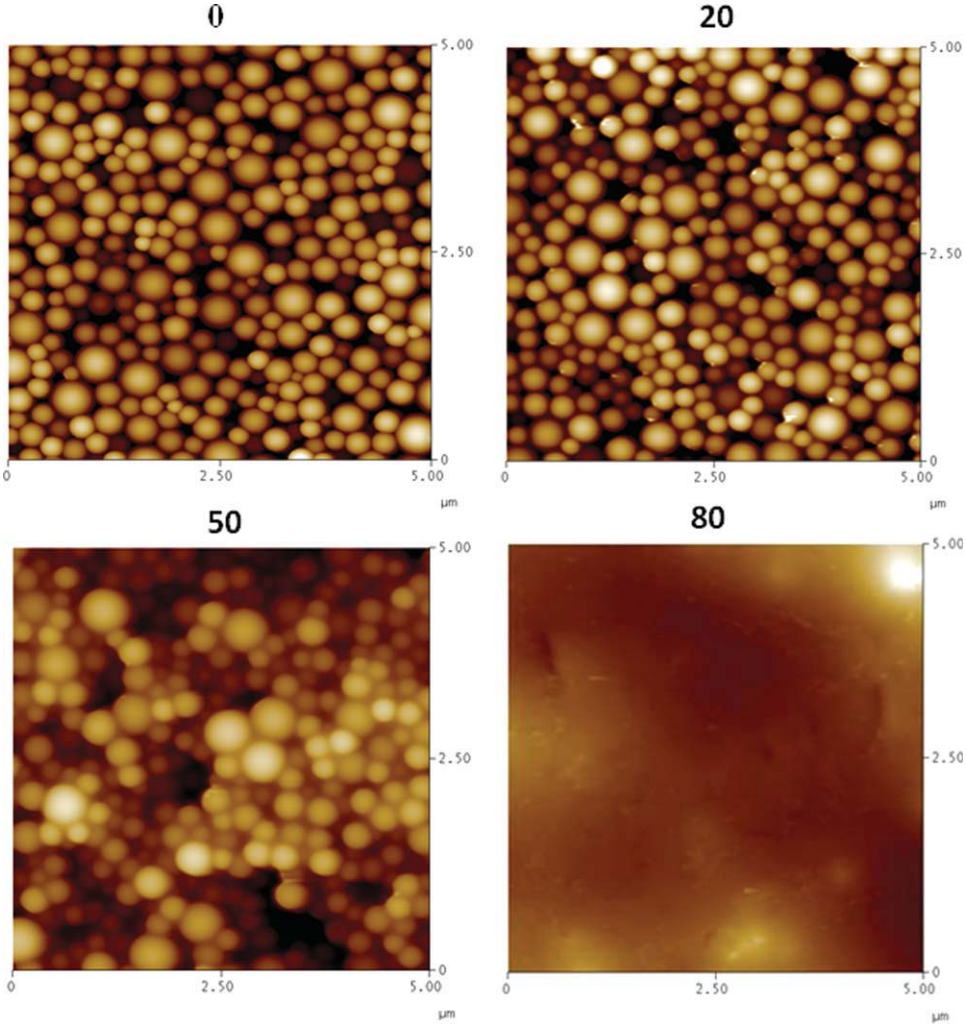

FIG. 14. AFM micrograph of 0, 20, 50, and 80 wt% PBA content blend films (Series 1) annealed at 100°C for 10 min. [Color figure can be viewed in the online issue, which is available at wileyonlinelibrary.com.]

LgPS particles (diameter 900 nm). As their total surface energy is much less than that of SmPS particles, LgPS particle requires higher energy to complete viscous flow process.

Healing and Interdiffusion

The decrease in I_P was already explained in previous section, by interdiffusion of polymer chains. As the annealing temperature is increased above maxima, some part of the polymer chains may cross the junction surface and particle boundaries disappear, as a result I_P decreases because of transparency of the film. To quantify these results, the Prager–Tirrell model [36, 37] for the chain crossing density can be used. In terms of reduced time $\tau = 2vt/N^2$, the total crossing density can be written as [31]

$$\sigma(\tau)/\sigma(\infty) = 2\pi^{-1/2}\tau^{1/2}, \tag{4}$$

where v and N are the diffusion coefficient and number of freely jointed segment of polymer chain [36].

The decrease in I_P in Figs. 5 and 6 above T_h is already related to the disappearance of particle–particle interface. As annealing temperature increased, more chains relaxed across the junction surface, and as a result the crossing density increases. Now, it can be assumed that I_P is inversely proportional to the crossing density $\sigma(T)$ and then the phenomenological equation can be written as

$$I_P(\infty) = R_0^{-1}\exp(\Delta E/2k_BT). \tag{5}$$

Here, ΔE is the activation energy for backbone and k is the Boltzmann constant. Logarithmic plots of I_P versus T^{-1} are presented in Figs. 10 and 11 for both series, respectively. The activation energy of backbone motion, ΔE is produced by fitting the data in these figures (the left-hand side) to *Eq. 5* and are listed in Table 2. Here, we have to mention that although the fitting seems much nicer for low PBA content films, the fits in Figs. 10 and 11 for high

 DOI 10.1002/pc

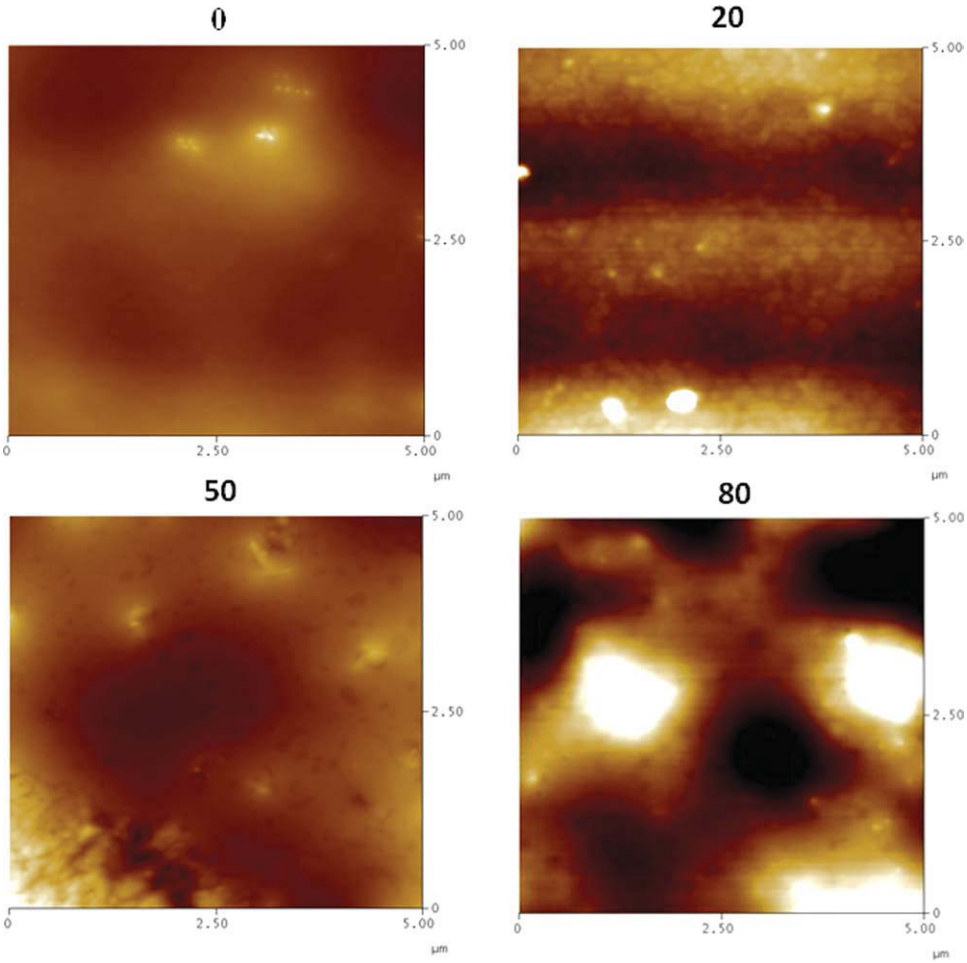

FIG. 15. AFM micrograph of 0, 20, 50, and 80 wt% PBA content blend films (Series 1) annealed at 150°C for 10 min. [Color figure can be viewed in the online issue, which is available at wileyonlinelibrary.com.]

PBA content films are not well behaved, that is, the model is probably not well suited to the data because of the phase separation process between PS and PBA phases in these films. ΔE value does not change with increasing PBA content for both series indicating that blend composition does not affect the backbone motion of the polymer chains across the junction surfaces. In addition, ΔE values are larger than the void closure activation energies for both series. This result is understandable because a single chain needs more energy to execute diffusion across the polymer–polymer interface than to be accomplished by the viscous flow process. Furthermore, ΔE values for LgPS/PBA series are larger than that of SmPS/PBA series. The polymer chains contain more free volume and less interactions between segments in SmPS chains leading to higher conformational energy and less interaction of polymer chains, which were confirmed by the solid-state NMR measurements and other methods [38, 39]. Polymer chains in the SmPS particle (diameter 320 nm) are in a highly confined state because of the spatial limitation compared to that of the random-coil state [38] in LgPS particles. This is the major reason for the SmPS particles need less energy to accomplish interdiffusion process in comparison with LgPS particles. These results are also in consistent with the results reported in literature. It has been found that a smaller particle-sized latex produces a faster rate of interparticle fusion, caused by the greater capillary force between the smaller particles [40]. Song et al. [41] showed that the surface molecular diffusion in the latex film is driven by the surface tension or surface free energy. Also, the interfacial capillary forces for smaller particles should be larger.

Minimum Film Formation and Healing Temperatures

An important characteristic related to the film formation properties of latexes is the minimum film formation temperature (T_0) and healing temperature (T_h). T_0 is commonly performed in the coatings industry and considered as the primary indicator of the lower temperature range over which a latex can be used in applications [2, 42, 43]. In other words, T_0 is often used to indicate the lowest possible temperature for particle deformation suffi-

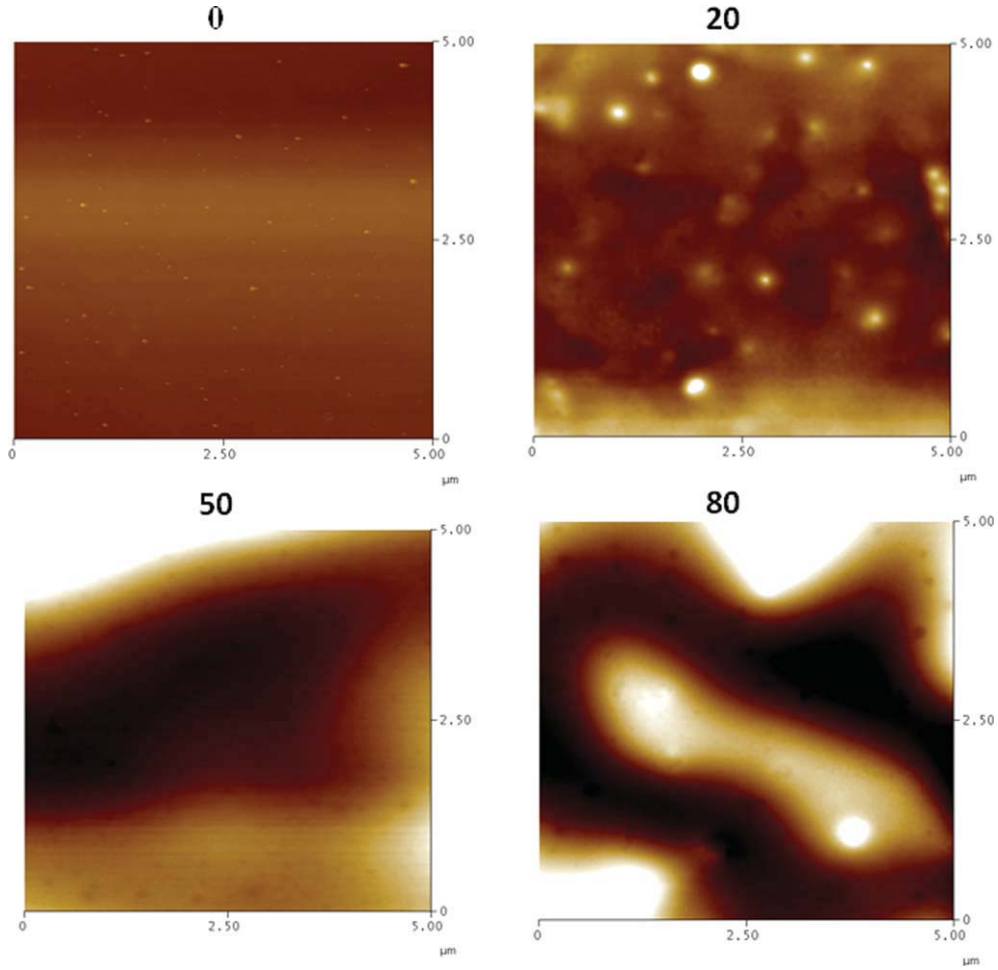

FIG. 16. AFM micrograph of 0, 20, 50, and 80 wt% PBA content blend films (Series 1) annealed at 200°C for 10 min. [Color figure can be viewed in the online issue, which is available at wileyonlinelibrary.com.]

cient to decrease interstitial void diameters to sizes well below the wavelength of light [44]. Below this critical temperature, the dry latex is opaque and powdery. However, at and/or above this temperature, a latex cast film becomes continuous and clear film [45]. Therefore, T_0 has been considered in this study as the temperature above which the I_{tr} starts to increase. The healing temperature (T_h) is the minimum temperature at which the latex film becomes continuous and free of voids. The healing point indicates the onset of the particle–particle adhesion [45]. Here, T_h is defined as the maxima of the I_P curves versus temperature.

The T_0 and T_h values measured for two latex blends series are reported in Table 3. From the table, the T_0 and T_h temperatures are about 110 and 130–150°C for the SmPS/PBA blends, 140–160 and 170–200°C for the LgPS/PBA, respectively. Although T_0 and T_h do not change so much within the each series with PBA content, both are shifted to higher temperatures with the size of hard PS. This points out that they were strongly influenced by the hard particle size. In other words, comparing to the LgPS/PBA blends, the film formation process of SmPS/PBA blends occurs at much lower temperature. This can be explained with the confined state of polymer chains with less interactions between segments leading to a higher conformational energy. Therefore, the film formation process is completed in much narrower temperature range for SmPS/PBA series driven mainly by the larger total surface energy. Previous workers [3, 46] have demonstrated that smaller particles have a lower minimum film formation temperature for these reasons. Moreover, Sperry et al.[3], using a geometric argument, have proposed that it should take a longer time for voids to close in a latex film based on larger particle sizes. In light of these past results and theoretical work [47], in latex dispersions of larger particles, poorer film formation and a greater void fraction at a given time are expected in comparison to an identical latex with smaller particles. Goudy et al. [48] reported that films composed of smaller latex particles (diameter: 240 nm) are more susceptible to fusion than those composed of larger latex particles (diameter: 375

 DOI 10.1002/pc

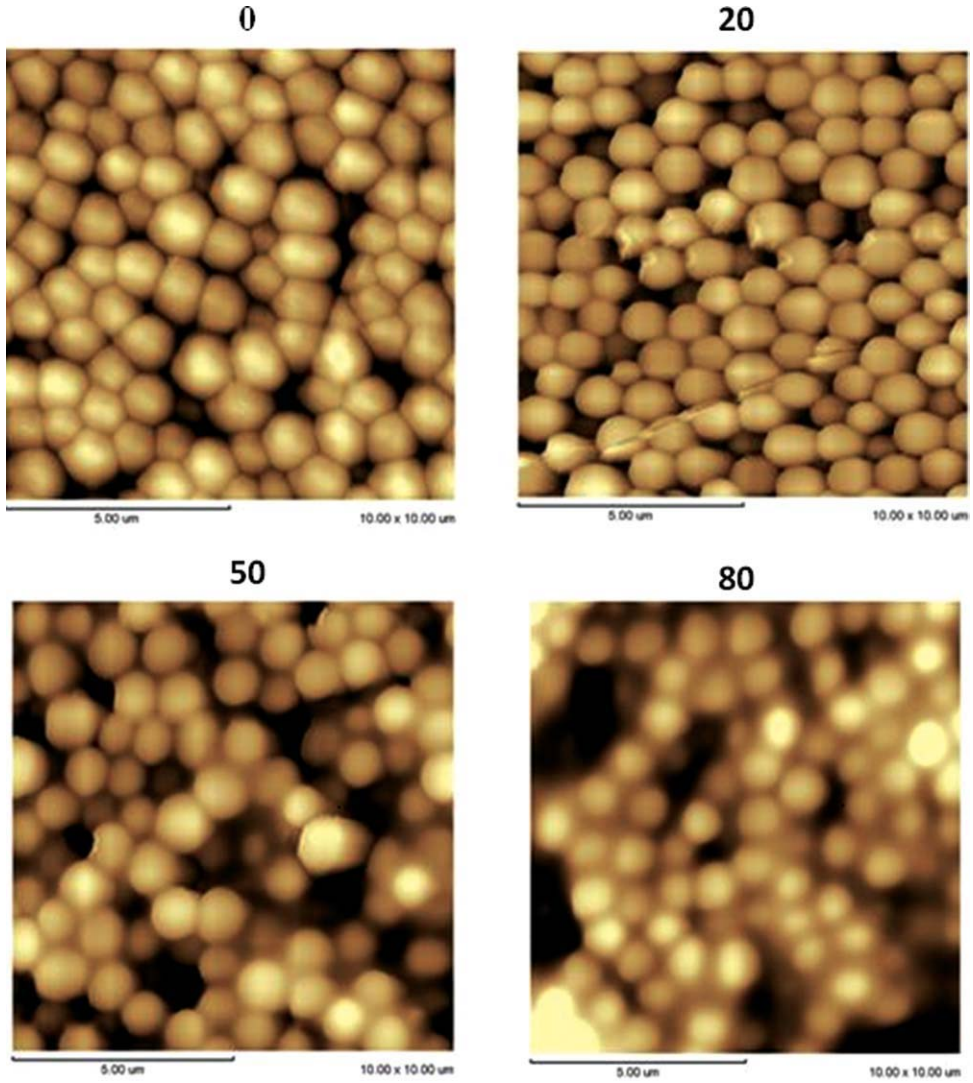

FIG. 17. AFM micrograph of 0, 20, 50, and 80 wt% PBA content blend films (Series 2) annealed at 100°C for 10 min. [Color figure can be viewed in the online issue, which is available at wileyonlinelibrary.com.]

nm). TMA measurements show that the sintering of nanoparticles (diameter 140 nm) was mostly completed within the temperature range of 70–90°C, whereas the sintering of larger particles requires higher temperature or longer time [49].

Film Morphology

In Figs. 14–16, we present AFM images of the blends for SmPS/PBA series, which have 0, 20, 50, and 80 wt% PBA contents at different annealing temperatures. At 100°C (see Fig. 14), no deformation in SmPS particles is observed. In Fig. 14a and b, at low PBA contents (0 and 20 wt%), the hard spheres seem to be randomly distributed and contain a lot of voids, which give highly opaque film. However, AFM images for 50 wt% PBA content film (Fig. 14c) show that the soft particles undergo complete coalescence and fill the voids between the hard SmPS particles with covering them. There is tendency for the hard SmPS particles to aggregate in these films. In Fig. 14d (80 wt% PBA content film), SmPS hard particles seem completely imbedded in the continuous phase generated by the soft latex. After annealing treatment at 150°C (see Fig. 15), AFM images clearly show the coalescence of SmPS particles for low PBA content films (Fig. 15a–c). Whereas for 80 wt% PBA film, almost no connection between small dispersed SmPS clusters in PBA matrix contribute to latex film formation, only they remain as individual coalesced domains. Upon annealing the films at 200°C, 0, 20, and 50 wt% PBA content films (Fig. 16a–c) show a more or less regular and continuous surface structures depending on the SmPS content in the blend. However, despite the smooth surface for 80 wt% PBA content film, surface morphology shows separated domains, which may be a sign for the phase separation process between PBA and SmPS polymers [50, 51].

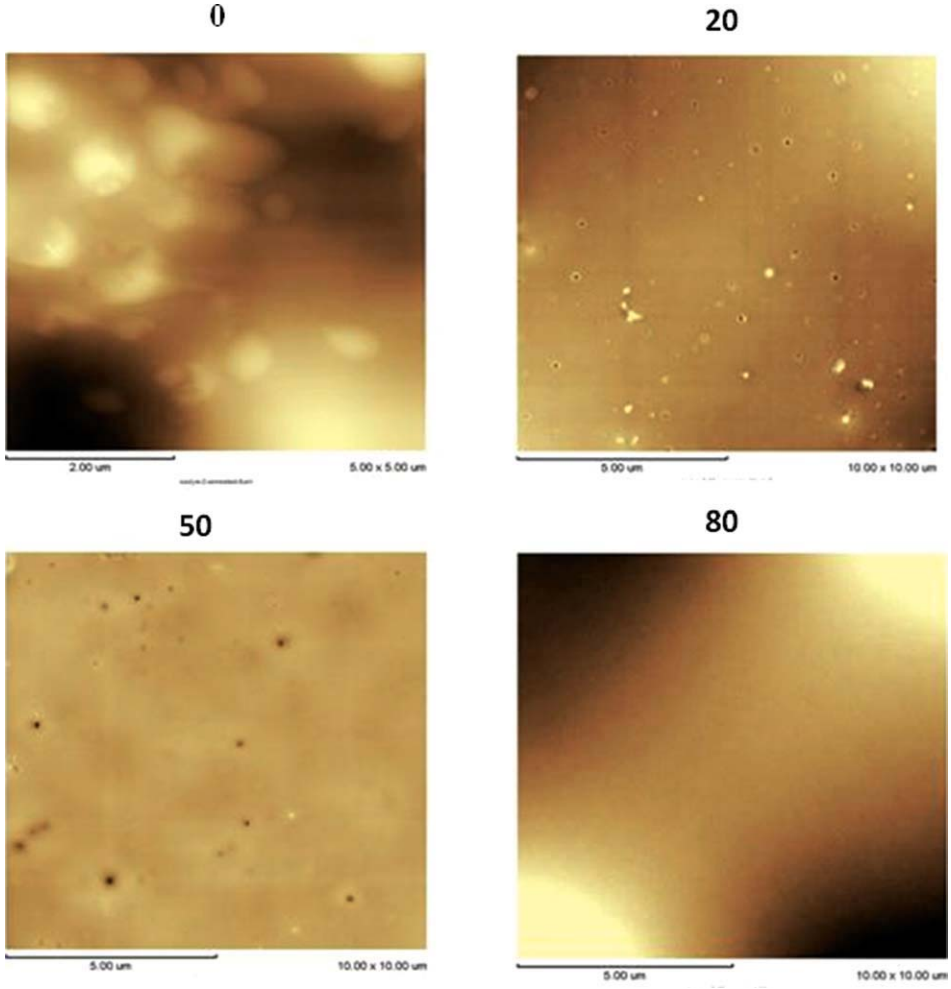

FIG. 18. AFM micrograph of 0, 20, 50, and 80 wt% PBA content blend films (Series 2) annealed at 150°C for 10 min. [Color figure can be viewed in the online issue, which is available at wileyonlinelibrary.com.]

The film formation process of LgPS/PBA blend was quit different from that of SmPS/PBA blend, as shown in Figs. 17–19. The contour of the LgPS particles is clearly seen in the images when the annealing temperature was 100°C (see Fig. 17). As can be seen in Fig. 17a, LgPS particles tend to cluster together to form close-packed domains for pure LgPS film. Additionally, at points of contact between particles, there is deformation from a spherical shape. Even so, particles retain their identity and do not reveal any significant changes in the surface morphology of the samples when compared with the AFM micrographs in Fig. 2b (dried pure LgPS film). In Fig. 17b–d for the PBA content films, the LgPS particles are seen well separated by the soft PBA particles with increasing PBA concentration. The close contact between the LgPS particles is seen only on rare occasions, especially when PBA content increases (Fig. 17c and d). The large particles appear for the most part in isolation rather than in clusters. This type of structure gives rise to relatively high average surface roughness. In blends containing LgPS particles, significant void content develops within clusters of the hard particles, which leads to lower I_{tr} values due to the light scattering from surface of the films in comparing with SmPS/PBA blend films (see Fig. 8).

Significant deformation of the LgPS contours in Series 2 is observed after annealing at 150°C (see Fig. 18). It has been indicated [52] that the greater the interdiffusion between polymer chains at the particle surface, the greater will be the loss of particle boundary. As seen in Fig. 18a, it must be noted that the particle's boundaries are still visible; this implies that the interparticle diffusion of polymer chains is limited after annealing at 150°C in pure LgPS film. However, PBA content film surfaces appear relatively smooth and flat revealing that the whole surface of these annealed films consists of a single phase. Figure 19 shows that the surface of films flattened completely after annealing at 200°C indicating that interdiffusion of the polymer chains and sintering take place to a certain extent. However, the contours of some number of LgPS particles remain discernible, as shown more clearly in the Fig. 19a, together with several homogeneous domains.

 DOI 10.1002/pc

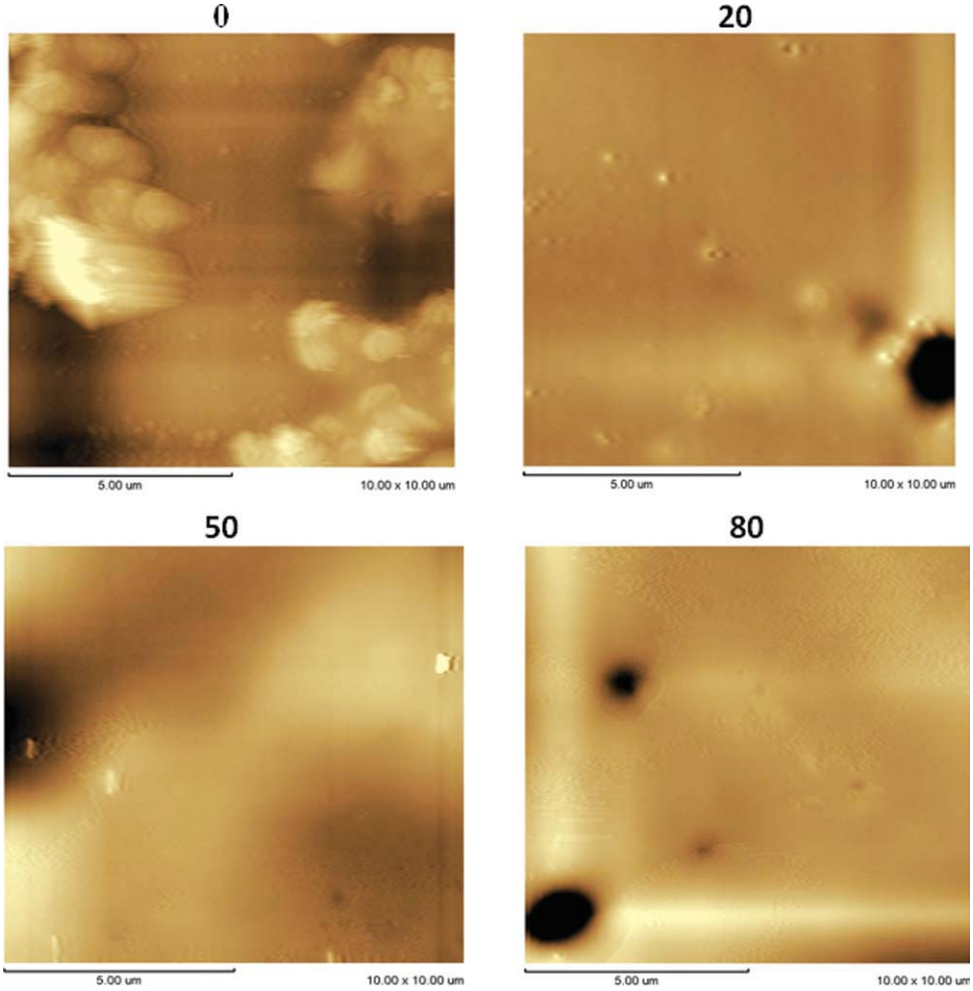

FIG. 19. AFM micrograph of 0, 20, 50, and 80 wt% PBA content blend films (Series 2) annealed at 200°C for 10 min. [Color figure can be viewed in the online issue, which is available at wileyonlinelibrary.com.]

However, in 20, 50, and 80 PBA content films, surface morphology shows spherical domains, which may be a sign for the spinodal decomposition process of this particular blend system [50, 51].

The AFM micrographs of the annealed sample clearly revealed (Figs. 14–19) that the hard particles had lost their initial spherical shape and formed a more or less continuous phase in soft PBA matrix depending on PS size. AFM micrographs also confirmed SSF and UVV data. It can be concluded that the morphology of the latex blends in two series progressively changed during annealing and affected by PS particle size.

CONCLUSIONS

The influence of composition and hard particle size on the film formation properties of hard/soft latex blends was investigated with SSF and UVV in support of the AFM. As soon as the thermal annealing temperatures become higher than T_g of the hard phase, the hard particles progressively lost their initial spherical shape and formed a more or less cocontinuous phase in the latex blends. Subsequently, it was concluded that as long as the weight fraction of the soft phase in the hard/soft latex blend did not exceed a critical value (R_c), PS particles percolate in PBA phase forming a continuous film. Above this critical value, the latex blend was no longer film forming at all temperatures. The critical weight fraction of soft particles (R_c) was presented as directly related to the hard particle size: the higher the hard particle size, the lower the critical weight fraction of hard particles leading to percolation. The AFM results are in excellent agreement with these results, we determined via SSF and UVV.

Compared to the LgPS/PBA blend, the sintering of SmPS/PBA blend occurred at much lower temperatures driven mainly by the larger total surface energy. It was also seen that energies required for void closure (ΔH) and interdiffusion (ΔE) processes in each series do not change with varying the blend composition. However, ΔH and ΔE values for SmPS/PBA were found to be less than that of LgPS/PBA series, which can be explained by the confined state of polymer chains with less interactions

between segments leading to a higher conformational energy.

REFERENCES

1. Th. Provder, M.A. Winnik, and M. Urban, Eds., *Film Formation in Waterborne Coatings, ACS Symposium Series*, Cambridge, 648 (1996).
2. J.L. Keddie, *Mater. Sci. Eng.*, **R21**, 101 (1997).
3. P.R. Sperry, B.S. Synder, M.L. O'Dowd, and P.M. Lesko, *Langmuir*, **10**, 2619 (1994).
4. S. Mazur, "Coalescence of Polymer Particles," in *Polymer Powder Processing*, N. Rosenweig, Ed., Wiley, New York, 157 (1995).
5. J.K. Mackenzie and R. Shuttleworth, *Proc. Phys. Soc.*, **62** (12-B), 838 (1949).
6. J.W. Vanderhoff, *Br. Polym. J.*, **2**, 161 (1970).
7. J.N. Yoo, L.H. Sperling, C.J. Glinka, and A. Klein, *Macromolecules*, **24**, 2868 (1991).
8. Ö. Pekcan, *Trends Polym. Sci.*, **2**, 236 (1994).
9. P.A. Steward, J. Hearn, and M.C. Wilkinson, *Adv. Colloid Interface Sci.*, **86**, 195 (2000).
10. M.A. Winnik and J.R. Feng, *J. Coat. Technol.*, **68**, 39 (1996).
11. S.T. Eckersly and B.J. Helmer, *J. Coat. Technol.*, **69** (864), 97 (1997).
12. J.F. Feng, M.A. Winnik, R.R. Shivers, and B. Clubb, *Macromolecules*, **28**, 7671 (1995).
13. R. Hagen, L. Salmen, O. Karlsson, and B. Wesslen, *J. Appl. Polym. Sci.*, **62**, 1067 (1996).
14. M.P.J. Heuts, R.A. Le Fêtre, J.L.M. Van Hilst, and G.C. Overbeek, *Am. Chem. Soc. Symp. Ser.*, **648**, 271 (1996).
15. D. Juhue and J. Lang, *Macromolecules*, **28**, 1306 (1995).
16. S. Lepizzera, C. Lhommeau, G. Dilger, T. Pith, and M.J. Lambla, *J. Polym. Sci. Part B: Polym. Phys.*, **35**, 2093 (1997).
17. R.M. Rynders, C.R. Hegedus, and A.G. Gilicinski, *J. Coat. Technol.*, **67** (845), 59 (1995).
18. D. Colombini, H. Hassander, O.J. Karlsson, and F.H.J. Maurer, *Macromolecules*, **37**, 6865 (2004).
19. S.T. Eckersley and B.J. Helmer, *J. Coat. Technol.*, **69**, 97 (1997).
20. J. Feng, E. Odrobina, and M.A. Winnik, *Macromolecules*, **31**, 5290 (1998).
21. A. Goudy, M.L. Gee, S. Biggs, and S. Underwood, *Langmuir*, **11**, 4454 (1995).
22. M.A. Winnik and J. Weng, *J. Coat. Technol.*, **66**, 99 (1996).
23. F.X. Chu, C. Graillat, and A. Guyot, *J. Appl. Polym. Sci.*, **70**, 2667 (1998).
24. W.B. Russel, D.A. Saville, and W.R. Schowalter, *Colloidal Dispersions*, Cambridge University Press, Cambridge, England (1989).
25. D. Colombini, H. Hassander, O.J. Karlsson, and F.H.J. Maurer, *J. Polym. Sci. Part B: Polym. Phys.*, **43**, 2289 (2005).
26. J.M. Geurts, M. Lammers, and A.L. German, *Colloids Surf. A*, **108**, 295 (1996).
27. J.S. Liu, J.F. Feng, and M.A. Winnik, *J. Chem. Phys.*, **101**, 9096 (1994).
28. F. Belaroui, B. Cabane, M. Dorget, Y. Grohens, P. Marie, and Y. Holl, *J. Colloid Interface Sci.*, **262**, 409 (2003).
29. Ş. Uğur, A. Elaissari, and Ö. Pekcan, *J. Colloid Interface Sci.*, **263**, 674 (2003).
30. Ş. Uğur, A. Elaissari, and Ö. Pekcan, *J. Coat. Technol. Res.*, **1** (4), 305 (2004).
31. Ö. Pekcan and E. Arda, *Colloids Surf. A*, **153**, 537 (1999).
32. G.H. Meeten, *Optical Properties of Polymers*, Elsevier Applied Science Publishers, London, 29 (1986).
33. L. Bohn, in *Polymer Handbook*, 2nd ed., J. Brandup and E.H. Immergut, Eds., Wiley-Interscience, New York (1975).
34. S.L. Rosen, *Polym. Eng. Sci.*, **7** (2), 115 (1967).
35. J.L. Keddie, P. Meredith, R.A.L. Jones, and A.M. Donald, *Langmuir*, **12**, 3793 (1996).
36. S. Prager and M. Tirrell, *J. Chem. Phys.*, **75**, 5194 (1981).
37. R.P. Wool, B.L. Yuan, and O.J. McGarel, *J. Polym. Eng. Sci.*, **29**, 1340 (1989).
38. C. Wu, K.K. Chan, K.F. Woo, R. Qian, X. Li, L. Chen, D.H. Napper, G. Tan, and A.J. Hill, *Macromolecules*, **28**, 1592 (1995).
39. X. Qu, Y. Tang, L. Chen, and X. Jin, *Chin. Sci. Bull.*, **46**, 991 (2001).
40. A. Goudy, M.L. Gec, S. Biggs, and S. Underwood, *Langmuir*, **11**, 4454 (1995).
41. M. Song, D.J. Hourston, H. Zhang, A. Hammiche, and H.M. Pollock, *Polymer*, **42**, 6299 (2001).
42. P.A. Steward, J. Hearn, and M.C. Wilkinson, *Adv. Colloid Interface Sci.*, **86**, 195 (2000).
43. D.P. Jensen and L.W. Morgan, *J. Appl. Polym. Sci.*, **42**, 2845 (1991).
44. J.L. Keddie, P. Meredith, R.A.L. Jones, and A.M. Donald, *Macromolecules*, **28**, 2673 (1995).
45. S.T. Eckersley and A. Rudin, *J. Coat. Technol.*, **62**, 89 (1990).
46. D.P. Jensen and L.W. Morgan, *J. Appl. Polym. Sci.*, **42**, 2845 (1991).
47. A.F. Routh and W.B. Russel, *Langmuir*, **15**, 7762 (1999).
48. A. Goudy, M.L. Gee, S. Biggs, and S. Underwood, *Langmuir*, **11**, 4454 (1995).
49. S. Mazur, R. Bacherbaner, and J. Buckholz, *Langmuir*, **13**, 4287 (1997).
50. I.S. Pollos, M. Soliman, C. Lee, S.P. Gido, K.S. Rohr, and H.H. Winter, *Macromolecules*, **30**, 4470 (1997).
51. T.K. Kwel, T. Nishi, and R.F. Roberts, *Macromolecules*, **7**, 667 (1974).
52. (a) M. Canpolat and Ö. Pekcan, *Polymer*, **36**, 2025 (1995); (b) M. Canpolat and Ö. Pekcan, *Polymer*, **38**, 2595 (1997).

 DOI 10.1002/pc